Aerosol-OT Reversed Micellar Formation at Low Water-Surfactant Ratio Studied by Synchrotron Radiation Small-Angle X-ray Scattering

ARTICLE *in* THE JOURNAL OF PHYSICAL CHEMISTRY · APRIL 1995

Impact Factor: 2.78 · DOI: 10.1021/j100017a056

9 AUTHORS, INCLUDING:

Mitsuhiro Hirai
Gunma University
98 PUBLICATIONS **1,183** CITATIONS

SEE PROFILE

Rika Hirai
Gunma University
23 PUBLICATIONS **408** CITATIONS

SEE PROFILE

Toshihiro Hirai
Shinshu University
197 PUBLICATIONS **1,460** CITATIONS

SEE PROFILE

Aerosol-OT Reversed Micellar Formation at Low Water-Surfactant Ratio Studied by Synchrotron Radiation Small-Angle X-ray Scattering

Mitsuhiro Hirai,*,† Rika Kawai-Hirai,‡ Sadato Yabuki,† Toshiharu Takizawa,† Toshihiro Hirai,⊥ Katsumi Kobayashi,∥ Yoshiyuki Amemiya,∥ and Masanao Oya‡

Department of Physics, Gunma University, Maebashi 371, Japan, Faculty of Engineering, Gunma University, Kiryu 376, Japan, Faculty of Textile Science and Technology, Shinshu University, Ueda 386, Japan, and National Laboratory for High Energy Physics, Tsukuba 305, Japan

Received: October 13, 1994; In Final Form: February 7, 1995[⊗]

By using synchrontron radiation small-angle X-ray scattering, we have studied the structure of biologial buffer/sodium bis(2-ethylhexyl)sulfosuccinate (AOT)/2,2,4-trimethylpentane (isooctane) reversed micelles with varying water-surfactant molar ratio ω_0 (=$[H_2O]/[AOT]$), AOT concentration, and temperature. The scattering data were analyzed by several methods, including a shell modeling. Although in a high ω_0 range ($16 < O_0 < 50$) the obtained structural parameters of the AOT reversed micelle and the linear relation between the water pool radius and the ω_0 value are mostly in agreement with those determined by other authors, for $0 < \omega_0 < 12$, however, discrepancies were found. These deviations can be understood by a transient oligomerization of reversed micelles, where with the increase of water content the micellar oligomerization proceeds successively from a metastable oligomeric phase to a stable monomeric phase through a transient phase. Increasing the AOT concentration and/or temperature reduced the reverse micellar dimension.

Introduction

From various points of view relating to physicochemical properties and phase behavior of the self-assembly of pseudo-atom systems and with possible future practical applications such as microreactors, numerous studies have been actively pursued on various reversed micellar systems, especially on sodium bis-(2-ethylhexyl)sulfosuccinate (AOT) reversed micelles.[1-3] Phase diagrams of AOT reversed micellar systems show that AOT molecules are soluble in various apolar solvents and form water in oil (w/o) microemulsions over a wide range of water-surfactant molar ratio $\omega_0 = [H_2O]/[AOT]$.[4-6] Understandings of the relationship between the reversed micellar structure and the water content are somewhat ambiguous in a low ω_0 range ($\omega_0 < \sim 10$). In this report we will present experimental results on the structural stability of a biological buffer/AOT/isooctane reversed micelles at low ω_0 value.

Neutron and synchrotron radiation sources have served as very powerful methods for structural studies. Numerous studies using neutron scattering on both biological and synthetic polymers have shown some attractive feasibilities of this method by using the so-called contrast variation method,[7-11] and actually this scattering technique has been preferred for use in studies of AOT reversed micellar structures.[12-19] There were only a few studies using the synchrotron radiation X-ray scattering method on AOT systems.[16,20] Although the structural change of AOT reversed micelles induced by elevating the ω_0 value are considered fundamentally to result from an increase of the water pool radius, the AOT reversed micellar formation at a low ω_0 value ($\omega_0 < 16$), especially occluding biological aqueous solvent, has remained ambiguous. A few experimental reports address a slight deviation from a well-known linear relation between the water pool and micellar radii at a low ω_0 value;[21,22] however, their data and analyses could not clarify directly this anomaly of the reversed micellar structure at a low ω_0 value. Such an ambiguity on the above point in the previous reports seems to be attributable to an inevitable experimental limitation in data statistics which occasionally occurs in the neutron scattering method in spite of a high availability for the structural analysis of materials consisting of components with different average scattering densities.

In the present experiments, we could clarify a structural ambiguity in AOT revered micellar formation at a low water content regime by using the synchrotron radiation small-angle X-ray scattering method. A high-intensity X-ray beam available from a synchrotron radiation source has enabled us to eliminate the strong background disturbance originating from an organic solvent, namely, isooctane, compared with the use of X-ray from a conventional source and even compared with that of neutrons. In this report we will focus on presenting the experimental results on the structure of the biological buffer/AOT/isooctane reversed micellar system at low water-surfactant molar ratios.

Experimental Section

Materials and Specific Gravity Measurements. Sodium bis(2-ethylhexyl)sulfosuccinate (AOT) was purchased from Nacalai Tesque Inc. and 2,2,4-trimethylpentane (isooctane) and *N*-(2-hydroxyethyl)piperazine-*N'*-(2-ethanesulfonic acid) (Hepes) from Wako Pure Chemical Industries Ltd. Other reagents with special grade were used. Water was purified by a Millipore system. The buffer solution (0.01 M Hepes/NaOH with 1 mM $CaCl_2$) was adjusted at pH 8.0. The reversed micellar solutions with different ω_0 values were prepared by injecting various amounts of the above buffer solution, sonicated for 10 min at 30 °C at 46 kHz by the ultrasonicator of Sibata Kagaku type CS-20, and centrifuged for 5 min at 3000 rpm at 25 °C to

* To whom correspondence should be addressed.
† Department of Physics, Gunma University.
‡ Faculty of Engineering, Gunma University.
⊥ Shinshu University.
∥ National Laboratory for High Energy Physics.
⊗ Abstract published in *Advance ACS Abstracts,* April 1, 1995.

0022-3654/95/2099-6652$09.00/0

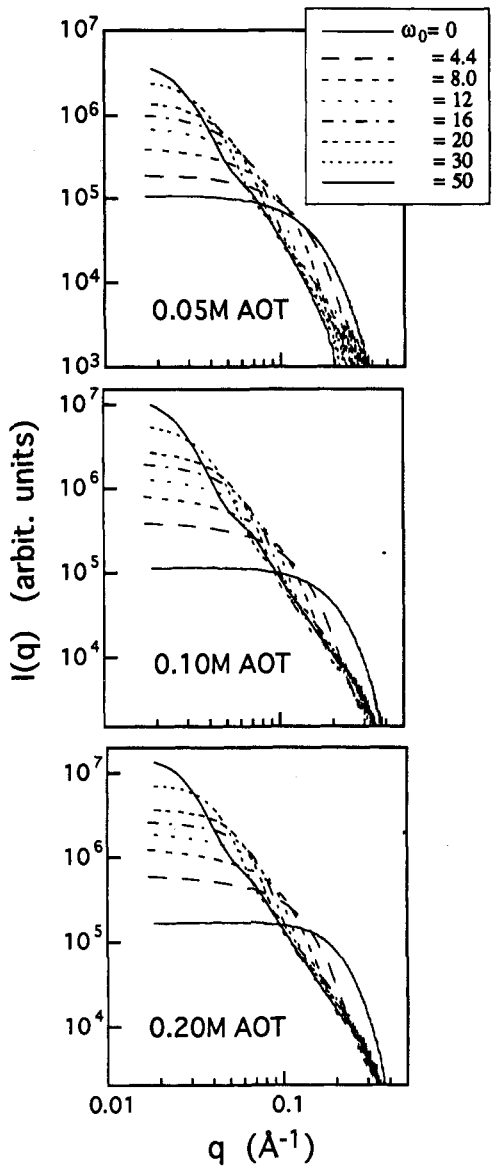

Figure 1. log $I(q)$ versus log q plots of the observed small-angle X-ray scattering profiles of AOT reversed micelles at 25.0 °C. The water–surfactant molar ratio ω_0 is varied from 0 to 50.

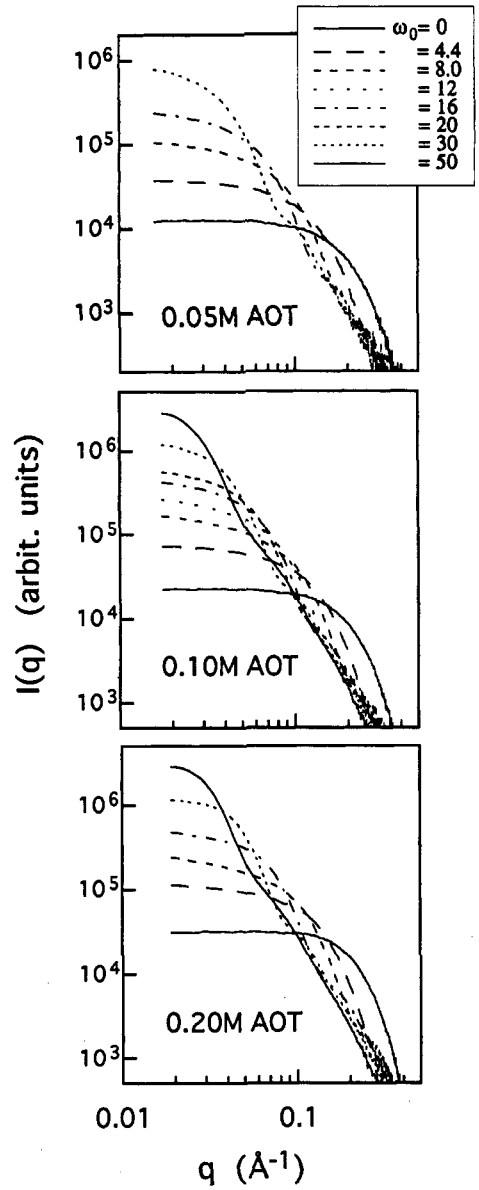

Figure 2. log $I(q)$ versus log q plots of the observed small-angle X-ray scattering profiles of AOT reversed micelles at 30.0 °C. The water–surfactant molar ratio ω_0 is varied from 0 to 50.

remove some large aggregates. After centrifugation the reversed micellar solutions were thermostated at 30 °C for 30 min and served for scattering measurements. Water contents in the reversed micellar solutions were determined by the Karl Fischer method using a Mitsubishi Kasei CA-05 moisture meter. By using a small pycnometer, specific gravities of the reversed micellar solutions at different temperatures (25, 30, and 35 °C) were measured to determine the specific volume per AOT molecule.

Small-Angle X-ray Scattering Experiments. Small-angle X-ray scattering measurements were performed by using a synchrotron radiation X-ray scattering spectrometer installed at the BL10C line of the 2.5-GeV storage ring in the Photon Factory of the National Laboratory for High Energy Physics, Tsukuba, Japan. The X-ray beam is monochromatized by using a double crystal monochromator and focused with a toroidal focusing mirror. Scattering data were recorded by using a one-dimensional position sensitive proportional counter with a 20-cm probe in effective length. The wavelength used was 1.49 Å, and the sample-to-detector distance was 87 cm. The details of the optics and instruments have been given elsewhere.[23] Samples were contained in a quartz cell with a 1-mm path length, and the temperature of the sample holder was maintained at 25.0 ± 0.1 or 30.0 ± 0.1 °C by circulating water. The exposure time was 480 s for each sample. The electron current in the storage ring was 250–350 mA.

Scattering Data Analysis. After correction of the scattering data by subtraction of the background noise, the following analyses were done. The beginning of the scattering profile $I(q)$ is known to depend on the Guinier equation in the form

$$I(q) = I(0) \exp(-q^2 R_g^2/3) \quad (1)$$

where $I(0)$ designates the zero-angle scattering intensity and R_g is the radius of gyration. By using the Guinier plot ($\ln(I(q))$ vs q^2) of the data sets in the small q range of 0.025–0.03 Å^{-1}, we determined the values of both $I(0)$ and R_g. The zero-angle scattering intensity $I(0)$ is proportional to the square of the total scattering amplitude I_{total}.[24]

For the middle scattering angle region, which is larger than the particle size ($qR_g \gg 1$) but smaller compared to typical chemical bond distances a ($qa \ll 1$), it is known that the

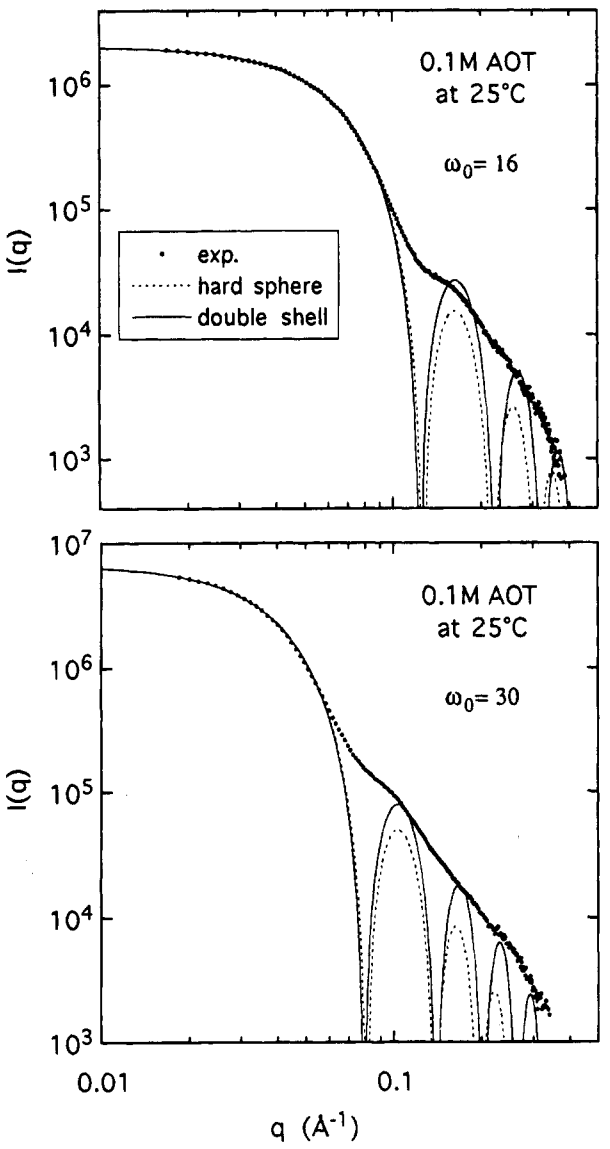

Figure 3. Spherical shell-model fitting of the observed scattering profiles. The difference of two types of model fittings using a hard sphere and a double-shell sphere. Each shell has a different scattering density, as shown in the text.

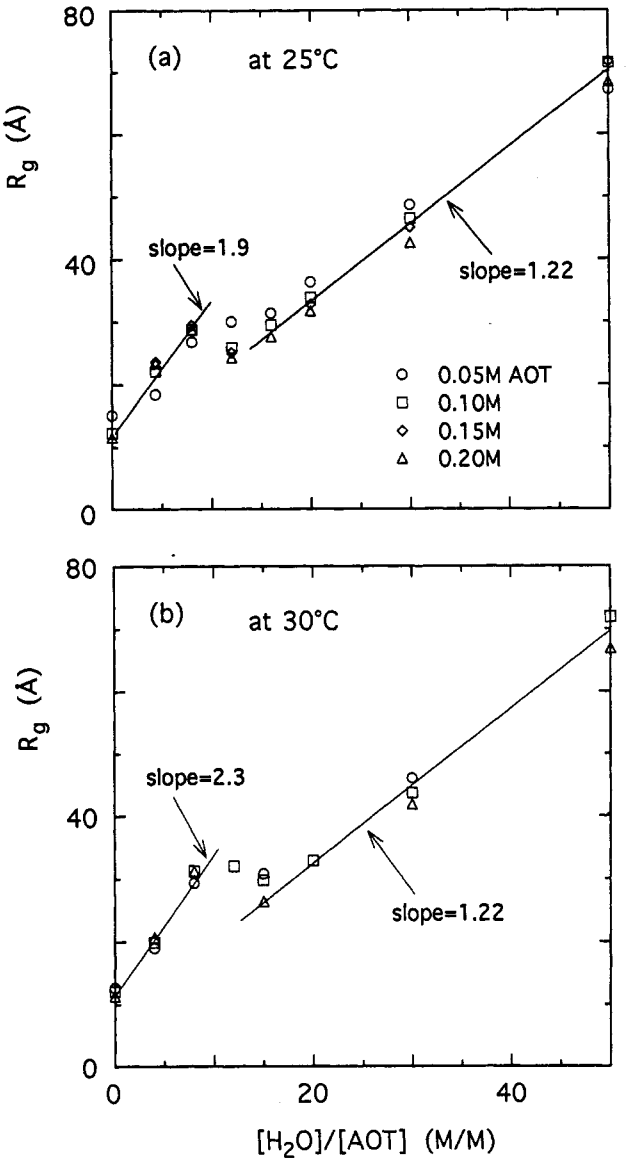

Figure 4. Dependence of the gyration radius of AOT reversed micelle on the water–surfactant molar ratio ω_0. a is at 25.0 °C and b at 30.0 °C. R_g values were estimated by the indirect Fourier transform method shown by Glatter.

scattering curves depend on the simple power low given by

$$\log I(q) = constant + \alpha \log q \qquad (2)$$

where α is the Porod slope. The evaluation of the Porod slope is useful in characterizing and ascertaining the geometric properties of random structures.[25-32]

The distance distribution function $p(r)$ was obtained by Fourier inversion of the scattering intensity $I(q)$ as

$$p(r) = \frac{2}{\pi}\int_0^\infty rqI(q)\sin(rq)\,dq \qquad (3)$$

The $p(r)$ function depends on the particle shape, on the intraparticle scattering density distribution, and on the interparticle translational correlation. To reduce the Fourier truncation effect on the calculation of the $p(r)$ function, the extrapolation of the small-angle data sets by using the least-squares method on the Guinier plot and the modification of the scattering intensity as

$$I'(q) = I(q)\exp(-kq^2) \qquad (4)$$

(k is the artificial damping factor) were done. The maximum diameter D_{max} of the particle was estimated from the $p(r)$ function, satisfying the condition $p(r) = 0$ for $r > D_{max}$.

As the use of the Guinier approximation inevitably leads to inherent systematic distortions and similar difficulties caused by concentration or aggregation effects, the following indirect Fourier transform method (the Glatter's method[33]) is useful in eliminating such artifacts for the estimation of R_g and I_{total}. These two terms are given as

$$I_{total} = \int_0^{D_{max}} p(r)\,dr \qquad (5)$$

$$R_g^2 = \frac{\int_0^{D_{max}} p(r)r^2\,dr}{2\int_0^{D_{max}} p(r)\,dr} \qquad (6)$$

Here we used the two different methods given above. Equation 5 was used for normalization of the $p(r)$ functions.

According to the convolution theory, the spherically averaged scattering function $I(q)$ from a particle composed of n shells with different average scattering densities is simply given as

$$I(q) \propto \langle A(\mathbf{q})\, A^*(\mathbf{q}) \rangle$$

$$= \int_0^1 [3\{\bar{\varrho}_1 V_1 j_1(qR_1)/(qR_1) + \sum_{i=2}^{n} (\bar{\varrho}_i - \bar{\varrho}_{i-1}) V_i j_1(qR_i)/(qR_i)\}]^2 \, dx \quad (7)$$

where $\langle\ \rangle$ means the spherical average of the scattering intensity $I(q)$ defined by $A(\mathbf{q})\, A^*(\mathbf{q})$ (the structural factor $A(\mathbf{q})$), $\bar{\varrho}_i$ is the average excess scattering density (so-called contrast) of the ith shell with a shape with an ellipsoid of rotation, and j_1 is the spherical Bessel function of the first rank.[34,35] R_i is defined as

$$R_i = r_i(1 + x^2(\nu_i^2 - 1))^{1/2} \quad (8)$$

where r_i and ν_i are the semiaxis and its ratio of the ith ellipsoidal shell, respectively. The radius of gyration R_g of this particle is given as

$$R_g^2 = [\nu_1(2 + \nu_1^2)\bar{\varrho}_1 R_1^5 + \sum_{i=2}^{n} \bar{\varrho}_i \{\nu_i(2 + \nu_i^2) R_i^5 - \nu_{i-1}(2 + \nu_{i-1}^2) R_{i-1}^5\}]/5\{\nu_1 \bar{\varrho}_1 R_1^3 + \sum_{i=2}^{n} \bar{\varrho}_i (\nu_i R_i^3 - \nu_{i-1} R_{i-1}^3)\} \quad (9)$$

Thus, for an nth layered sphere ($\nu_i = 1$), the R_g is simplified as

$$R_g^2 = \frac{3\{\bar{\varrho}_1 R_1^5 + \sum_{i=2}^{n} \bar{\varrho}_i (R_i^5 - R_{i-1}^5)\}}{5\{\bar{\varrho}_1 R_1^3 + \sum_{i=2}^{n} \bar{\varrho}_i (R_i^3 - R_{i-1}^3)\}} \quad (10)$$

Equation 10 can be used to simulate the gyration radius of AOT reversed micelle when the water pool radius and AOT molecular dimension are varied.

Results and Discussion

Scattering Profile Analysis. Figures 1 and 2 show the scattering profiles of the AOT reversed micelles at different temperatures (25.0 and 30 °C), where the water−surfactant molar ratio ω_0 was varied from 0 to 50. In the medium q region of 0.1−0.2 Å^{-1}, every scattering profile has a broad shoulder which can be attributed to the globular structure of the reversed micelles. With an increasing ω_0 value, the shoulders shift to low q and the scattering intensities in the small q region below 0.03 Å^{-1} increase significantly. These systematic variations evidently result from the enlargement of the micellar dimension induced by an injection of water. As shown in Figure 3, where we assumed a spherical shape for a micellar structure, the experimental scattering profiles are well fitted by a shell modeling using eq 7. The least-squares fitting parameters in this figure are a zero-angle scattering intensity and a micellar radius for both a hard sphere model and a double-shell sphere model. The outer-shell width corresponding to the total length of the AOT molecule is fixed at 12 Å. The average excess scattering densities of a double-shell sphere are given as $\bar{\varrho}_{AOT} = 4.2 \times 10^{-10}$ cm^{-2} and $\bar{\varrho}_{core} = 2.6 \times 10^{-10}$ cm^{-2}, respectively. These values are obtained experimentally by the following specific gravity measurements. It is evident that by considering a scattering density distribution of the AOT reversed micelles inside, we can qualitatively fit the experimental scattering profiles much better, especially those at low ω_0 values.

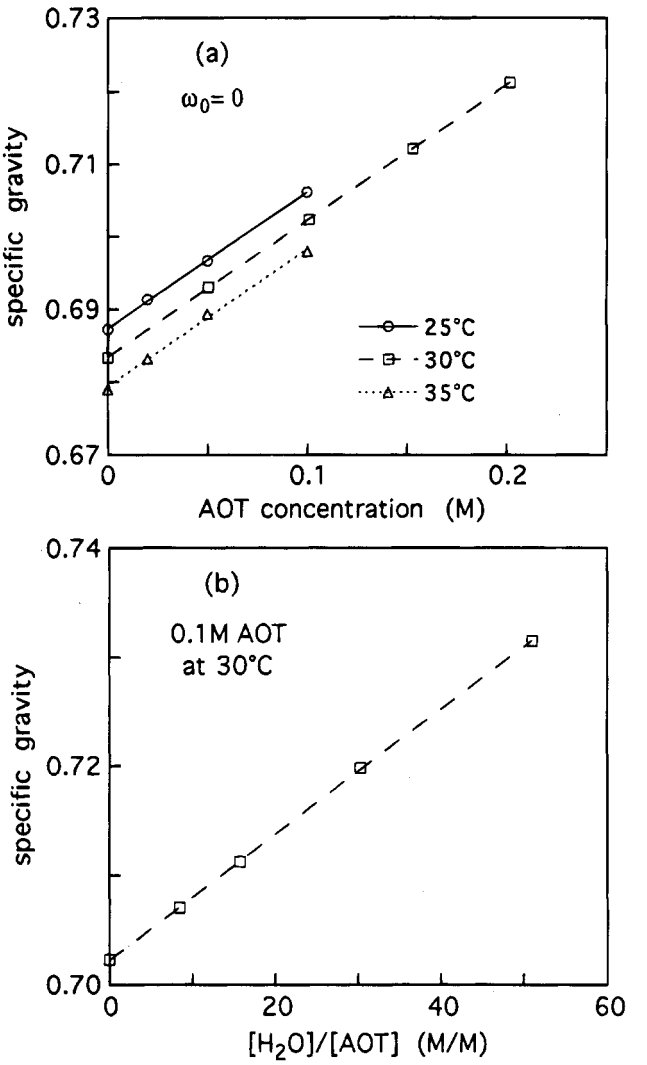

Figure 5. Dependence of the specific gravity of the AOT reversed micellar solution on AOT concentration (a) at 25, 30, and 35 °C and on water−surfactant molar ratio ω_0 (b) at 25 °C, 0.1 M AOT.

Thus, the smeared experimental $I(q)$ profile at the high q region mostly above 0.1 Å^{-1} suggests the presence of polydispersity of the micellar structure in dimension and shape.

The temperature difference induces a slight change of the slope in the middle scattering angle region, so-called the Porod regime. In the present case it can be thought that the change of the Porod slope in the q range higher than the shoulder position reflects the variation of the reversed micellar surface. When varying the ω_0 value from 12 to 50, the slope changes from −3.88 to −3.18 in Figure 1 and from −3.96 to −3.56 in Figure 2. This implies that by increasing the water content, the reversed micellar interface changes from a smooth surface (the slope is −4) to a fractally rough surface (the slope is in the range from −3 to −4). The interface tends to become more smooth by elevating the temperature from 25 to 30 °C. The above change in the Porod slope shows that the reversed micellar interface is sensitive not only to the water content but also to the temperature. The above discussions are supported by the following analyses.

Gyration Radius and Specific Gravity. By using the Guinier and Glatter methods based on eq 1 and 6, the gyration radius R_g of the reversed micelle was estimated. The latter method is known to be insensitive to the termination of $I(q)$ at a very small angle; therefore the accuracy of the determination of R_g is higher than that determined by using the former method. The ω_0 dependence of the gyration radius estimated by the

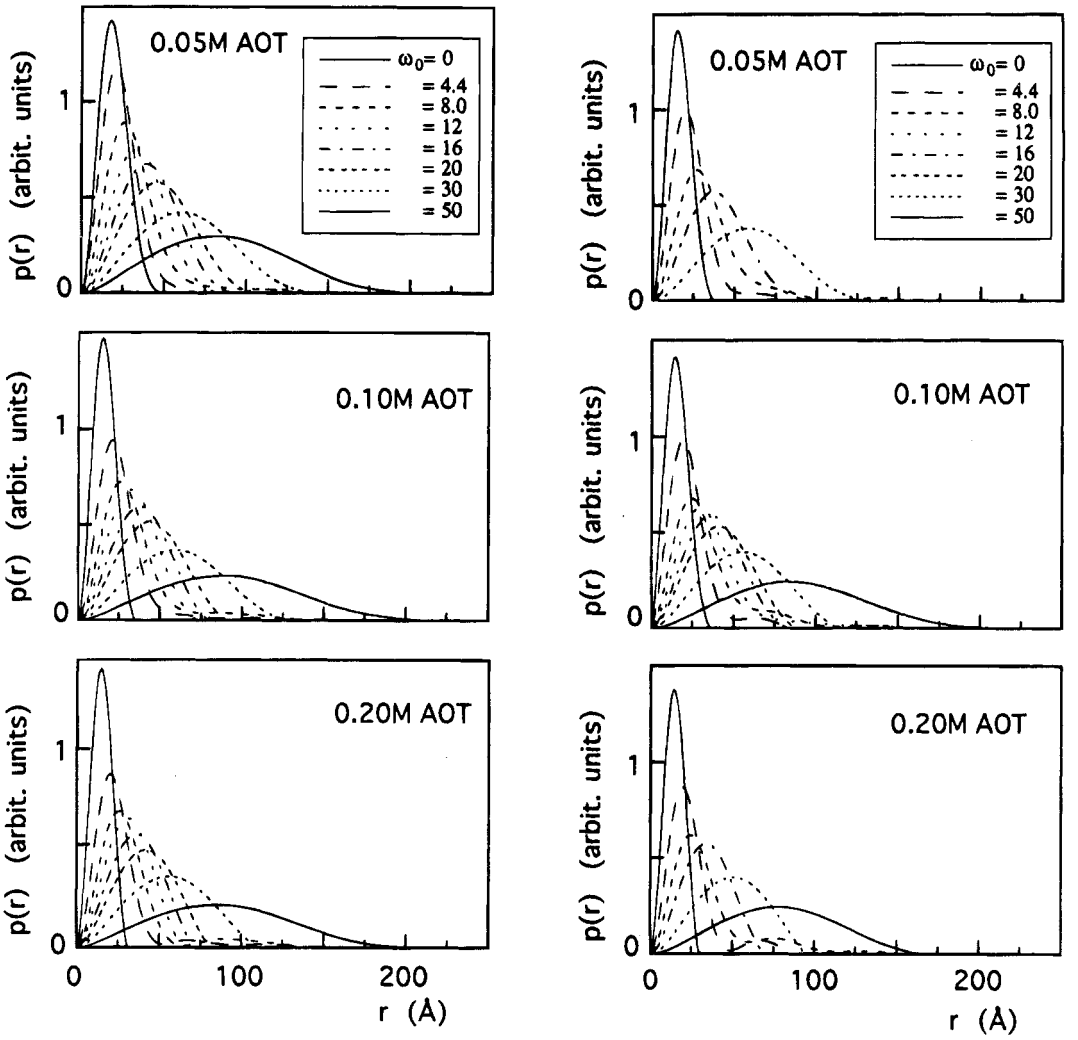

Figure 6. Variation of the distance distribution function $p(r)$ of the AOT reversed micelle as a function of the water−surfactant molar ratio ω_0. $p(r)$ functions in a (left column of panels) and b (right column of panels) were calculated from the scattering profiles in Figures 1 and 2, respectively. Each $p(r)$ function is normalized by the total scattering power.

Glatter method is shown in Figure 4a,b. The increasing tendency of R_g with an increase of ω_0 is evident, and we can distinguish three different regions in both panels of the figure, that is, the steep increasing region ($0 < \omega_0 < 8$), the mostly constant or slight decreasing region ($8 < \omega_0 < 16$), and the slow increasing region ($16 < \omega_0 < 50$). The slopes in the first and the third regions are indicated in the figure.

The water pool radius r_w of the AOT reversed micelle has been considered to depend on the relation of $r_w = 1.5\omega_0$ Å, which was derived from geometric consideration of the dimension and packing of AOT molecules.[36-38] On the basis of this relation, the R_g of the reversed micelle as a hard sphere with a homogeneous scattering density distribution inside depends on the relation of $R_g = (3/5)^{1/2}(r_w + l) \sim 1.16\omega_0 = 0.78l$ Å, where l is the total length of an AOT molecule. The slopes estimated in the third region ($16 < \omega_0 < 50$) is slightly larger than 1.16, indicating that a hard sphere model is too simple to describe the variation of R_g. By applying eq 10, we can estimate the R_g of a double-shell sphere model composed of a shell and a core with different average scattering densities, which is apparently more realistic than a hard spherical model. For this estimation the excluded volume of the AOT molecule must be known. This value was measured by the specific gravity measurements with varying AOT concentration and the ω_0 value at 25, 30, and 35 °C, as shown in Figure 5a,b. The dependence of the specific gravity both on the AOT concentration and on the ω_0 value shows good linearity, indicating that the excluded volume of AOT molecule is independent of both these values and just depends on temperature. From the slopes in Figure 5a we can estimate the specific volume per AOT molecule by using the following equation defined as

$$V_t^{AOT} = (M_{AOT} - 10^3\alpha)V_t^{iso}/M_{iso} \qquad (11)$$

where α is the slope, V_t^{AOT} and V_t^{iso} are the volumes of AOT and isooctane molecules at t (°C), and M_{AOT} and M_{iso} are the molecular weights. V_t^{iso} also depends on the temperature, whose values were measured to be 276.5 Å^3 at 25 °C, 277.6 Å^3 at 30 °C, and 279.3 Å^3 at 45 °C. By using eq 11 the volume of AOT molecule were obtained to be 622.1 Å^3 at 25 °C, 624.2 Å^3 at 30 °C, and 626.8 Å^3 at 35 °C. The average excess scattering densities of the AOT shell and of the water pool core in comparison to isooctane, the solvent, were estimated as $\bar{\varrho}_{AOT} = 4.2 \times 10^{-10}$ cm^{-2} and $\bar{\varrho}_{core} = 2.6 \times 10^{-10}$ cm^{-2}, respectively. Then, by using eq 10 on the assumption that $r_w = 1.5\omega_0$ Å and $l = 12$ Å, we can simulate the relation between R_g and ω_0 to be proportional to $1.22\omega_0 + 9.32$ Å. This relation well describes the experimental slope of $\omega_0 > 16$ in Figure 4. By applying the same equation to the R_g data sets in the third region ($16 < \omega_0 < 50$), we can estimate directly the relation between the water pool radius and the ω_0 ratio ($r_w = \alpha\omega_0$). The result of the least-squares fitting gives the α value of 1.50 ± 0.03, which is in good agreement with the theoretical value of 1.5 confirming the availability of the experimental R_g values

and the analysis presented above. It can be assumed that in the third region the change of the AOT reversed micellar structures proceeds by the simple enlargement of the water pool radius with an increase of ω_0.

For $0 < \omega_0 < 8$, R_g changes much more rapidly with ω_0. It is evident that such an ω_0 dependence of R_g is not explained by considering a deformation of the micellar structure from a spherical shape because the experimental data cannot be fitted by assuming an elongated ellipsoid model. However, the formation of the reversed micellar oligomers, where a small amount of oligomers results in a great increase of R_g, can provide an explanation of the anormalous ω_0 dependence of R_g in this ω_0 region. For example, the R_g of a dimer is 2.1 times larger than that of a monomer, even when the relation on the water pool radius holds and the micellar structures are identical spheres. As the R_g obtained experimentally is known to be a z-averaged mean-square value, a minor presence of micellar oligomers is expected to strongly increase the R_g value, which is also suggested by the following analyses. Hereafter, we will call this anomalous steep increasing region ($0 < \omega_0 < 8$) as a metaphase of the reversed micellar oligomerization and distinguish from the well-known monomeric phase holding the simple linear relation between R_g and ω_0.

Distance Distribution Analysis. By using the Fourier inversion with eqs 3−5, the distance distribution functions $p(r)$ were obtained, as shown in Figure 6a,b. The $p(r)$ functions, except for low ω_0 values (4.4 and 8), are characterized by a symmetrical bell-shaped peak. The slight tailing to a large r value for $\omega_0 \geq 30$ can be assumed to result from a minor polydispersity of the reversed micellar structure. In the case of a spherical particle the peak position p_{max} of the $p(r)$ function coincides with the radius of this particle, namely, in the present case a real radius R of the reversed micelle. The p_{max} values are plotted respectively in Figure 7a,b as a function of the ω_0 value. Every plot for different AOT concentrations shows good linearity and has a slope of 1.4−1.5 in the whole ω_0 range, indicating the change of the micellar radius was simply caused by the linear enlargement of the water pool radius with an increase of ω_0. The linear least-squares fits of the data yield an intercept, corresponding to the average radius at $\omega_0 = 0$ of 16.16 ± 0.03 Å. This value for a dry AOT reversed micelle is in good agreement with that (16.4 Å) obtained by considering a icosahedral packing of a AOT polar head with neutron scattering data.[39] On the other hand the $p(r)$ functions at $\omega_0 =$ 4.4 and 8 have low shoulders or humps which appear near double the distance of the bell-shaped main peak position. As the p_{max} values at both of these ω_0 values is also subject to the above linear relation, the appearance of the shoulders at these ω_0 values suggests a minor presence of reversed micellar oligomers, especially of dimers and trimers, attributing to the steep increase of the R_g value in these ω_0 ranges, as shown above. The maximum diameter D_{max}, meaning the longest length of the intraparticle vector of the solute particle, was obtained from the zero-cross point at a longer distance in the $p(r)$ function. The obtained D_{max} values are plotted as a function of the ω_0 value in Figure 8a,b. With elevation of the ω_0 value, the D_{max} value increases significantly at first in the metaphase, decreases abruptly at $\omega_0 = 16$, and gradually increases again. The fast increase of D_{max} in the ω_0 range from 4.4 to 8 is attributable to an occurrence of oligomeric particle formation. The following abrupt decrease in the ω_0 range around 10−16 can be explained as follows: the formation of the oligomeric reversed micelles decreases to reach a thermal equilibrium state where monomeric structures are rather stable. For a simple hard sphere D_{max} is twice that of p_{max}. In the high ω_0 range ($\omega_0 >$ 16), D_{max} gradually becomes greater than $2p_{max}$ with increasing ω_0. This suggests that the distortion of the micellar structure from a spherical shape was gradually induced by increasing ω_0, which can be related to the change in the Porod slope in Figures 1 and 2.

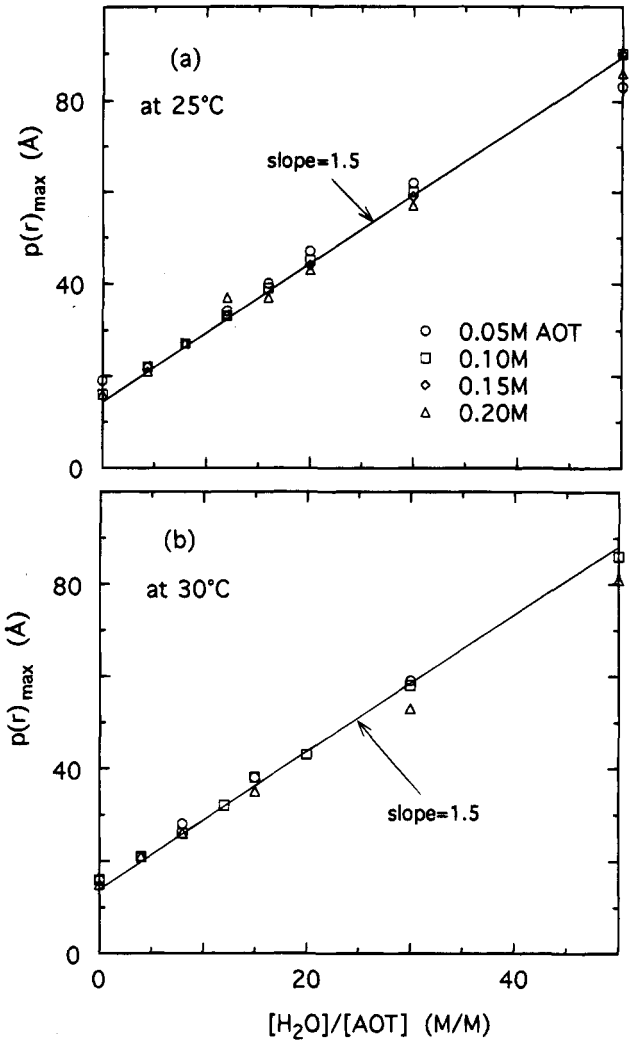

Figure 7. Plots of the peak position p_{max} as a function of the water−surfactant ratio ω_0. a and b correspond to 25.0 and to 30.0 °C in Figures 5, respectively.

As shown in Figure 9, the increase of the AOT concentration evidently causes a decrease of p_{max} and D_{max} values, indicating that the reversed micelles tend to form more compact structures. In Figure 10, the elevation of temperature shows mostly the same kind of effect on the micellar structure at high ω_0 ($\omega_0 >$ 20) and at a dry micellar state ($\omega_0 = 0$). AT ω_0 values ($\omega_0 <$ 16) except that of $\omega_0 = 0$, namely, at the metaphase (the oligomeric and following transient phases), the difference of the $p(r)$ profile is clearly seen in Figure 10, suggesting that the oligomerization is more evident at 30 °C than at 25 °C. Both factors, AOT concentration and temperature, can be thought to vary the ratio between the AOT molecular volume and the surface area of the AOT head polar group, resulting in a change of the radius of curvature of the reversed micelle.

Conclusion

In conclusion, by using synchrotron radiation small-angle X-ray scattering, we could clarify an ambiguity of the AOT reversed micellar structure at low water contents with varying water−surfactant molar ratio ω_0 and AOT concentration. According to the $p(r)$ function analysis, the p_{max} value, which

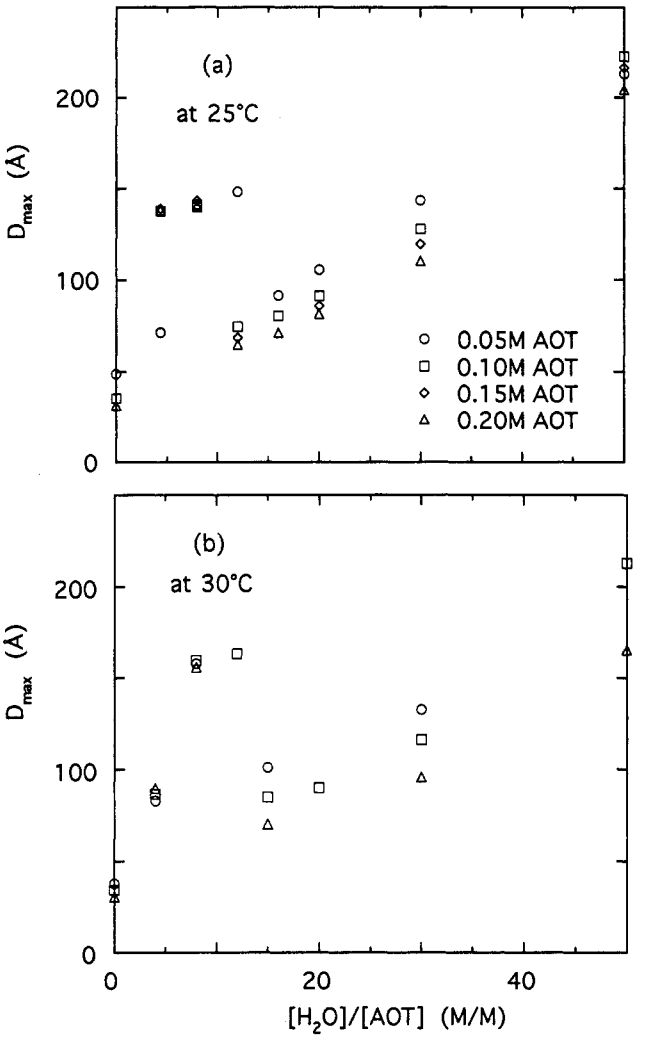

Figure 8. Plots of the maximum diameter D_{max} as a function of the water–surfactant ratio ω_0. a and b correspond to 25.0 and to 30.0 °C in Figures 5, respectively.

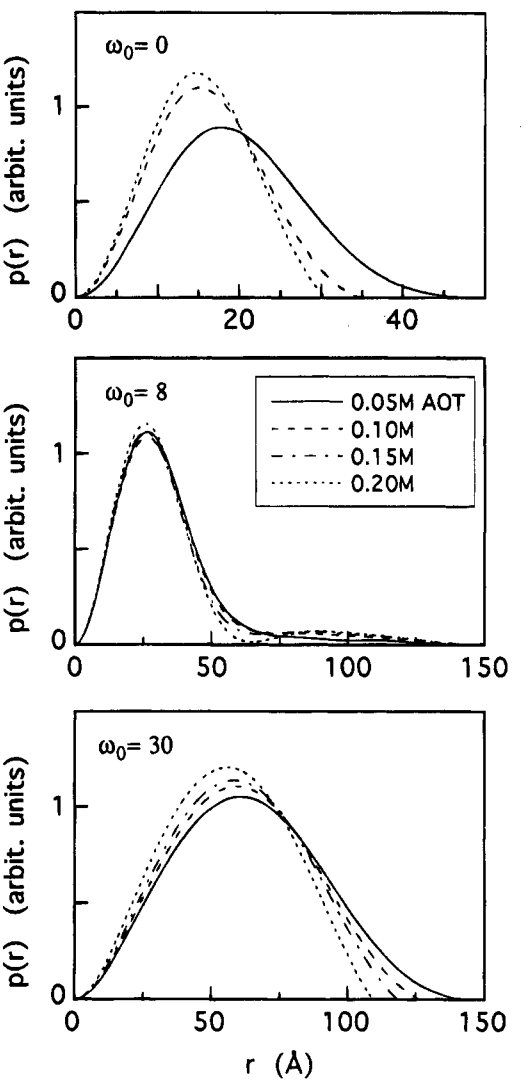

Figure 9. Dependence of the distance distribution function $p(r)$ at 25 °C on AOT concentration.

corresponds to the radius of the reversed micelle, shows the linear relation between the p_{max} and ω_0 values in the whole ω_0 range ($0 < \omega_0 < 50$). Its obtained slope is about 1.4−1.5 which mostly agrees with that of a well-known linear relation (the slope is 1.5) derived from geometric consideration of AOT reversed micellar structures. On the contrary, we have found the relation between the gyration radius R_g and the ω_0 value is much different from those shown in previous works and can evidently separate three different regions in the ω_0 value. Although the linear relation between R_g and ω_0 only holds in the high ω_0 region ($\omega_0 > 16$), its slope is much smaller than 1.5, as shown previously. The slope for a simple hard sphere is given apparently to be 1.16, and the slopes obtained are slightly larger than this value, which can be well explained by modeling analysis using a sphere with a heterogeneous scattering density distribution inside. In the medium ω_0 region ($8 < \omega_0 < 16$) the slope becomes mostly flat, and in the low ω_0 region ($\omega_0 < 8$) it becomes much steeper than that in the high ω_0 region. In combination with the $p(r)$ function analysis on the p_{max} and D_{max} values, we can describe these low and medium ω_0 regions as a metastable oligomeric phase and a transient phase from oligomers to monomers, respectively. These two phases, called a metaphase, have not been mentioned previously. Thus, the AOT reversed micellar formation can be assumed to proceed successively from a metastable oligomeric phase to a stable monomeric phase through a transient phase. The ω_0 value of those phase transitions is not so critical but almost independent of the AOT concentration at both temperatures of 25 and 30 °C. We have also found the effect of AOT concentration and temperature on the micellar structure. Both factors slightly reduce the reversed micellar dimension under the present sample condition. The formation of transient oligomers at a metaphase and the AOT concentraion dependence of the micellar dimension, as mentioned above, might be explained by assuming attractive interactions between AOT reversed micelles, such as an attractive square-well potential[40] or a sticky hard sphere potential;[41] however, the monomeric phase of the reversed micelles above $\omega_0 = 20$ cannot. On the other hand, a recent structural study of the water/cyclohexane/$Co(AOT)_2$ system suggests the phase transition of reversed micellar shape from spheres to cylinders at $\omega_0 = 0-10$ and from cylinders to spheres at $\omega_0 = 10-25$.[42] Such structural changes are well-known to greatly vary scattering and distance distribution function profiles;[9,32] however, they did not show any distance distribution function or R_g value dependence on ω_0. The present experimental results of the biological buffer/isooctane/Na(AOT) system does not show any evidence accompanied by such a transition. The oligomeric micellar formation found here might be attributable to a cylindrical micellar phase in another system. By the way, we have also studied the relation between the structure and reactivity of AOT reversed micelles entrapping α-chymotrypsins with varying ω_0 value, protein concentration, and substrates,[43] whereupon we have found a significant

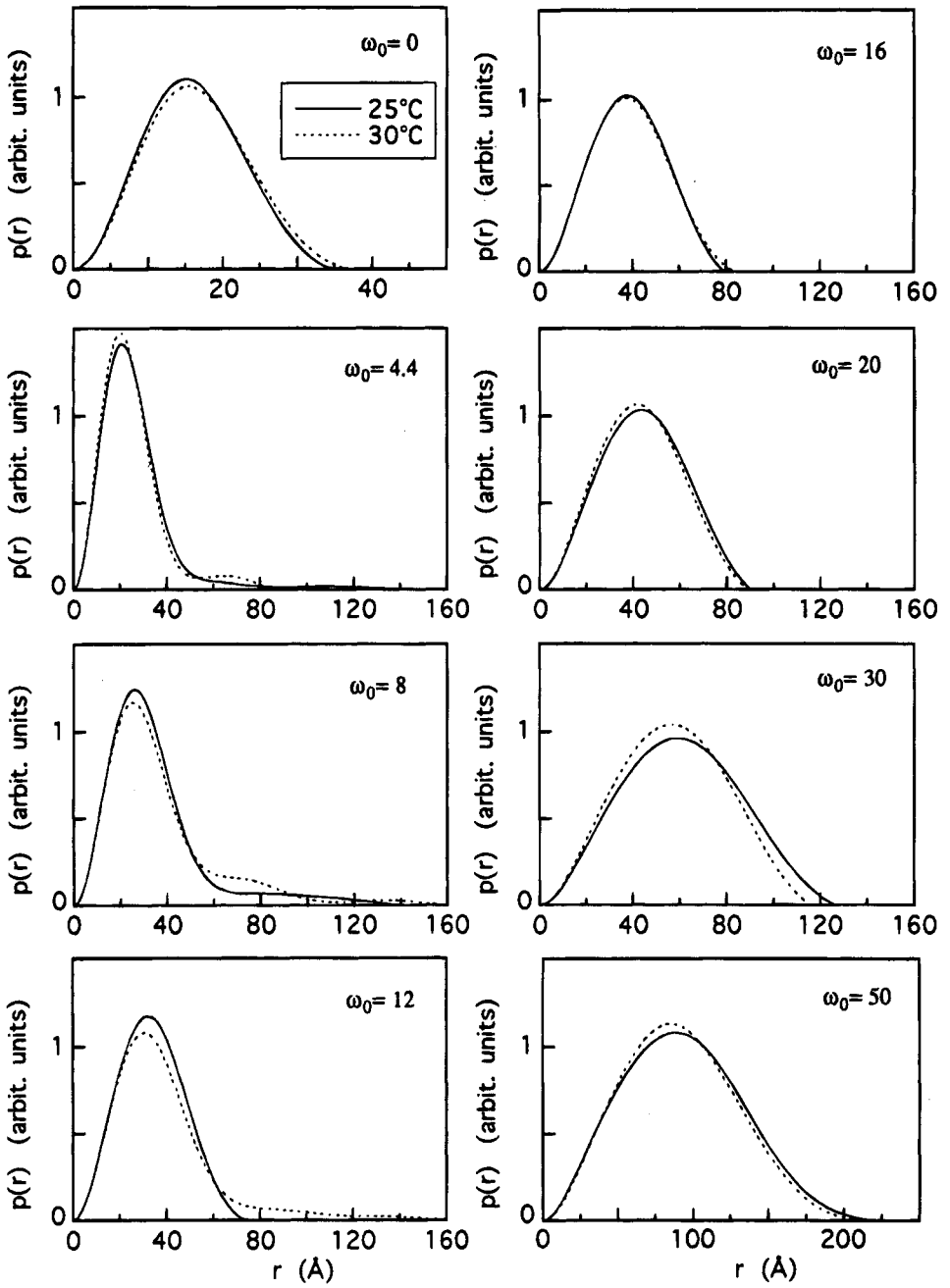

Figure 10. Change of the distance distribution function $p(r)$ of 0.1 M AOT by a temperature difference.

enhancement of the enzymatic activity in the low ω_0 range, namely, a typical bell-shaped-type enhancement with the maximum activity at $\omega_0 \sim 12$. For some enzymes the metastable oligomeric phase and the following transient phase seem to play an important role in accelerating a metabolic turnover by increasing an apparent interfacial area of reversed micelles being accessible closely to the enzymes.

Acknowledgment. This work was performed under the approval of the Photon Factory Program Advisory Committee of the National Laboratory for High Energy Physics (Proposal No. 94G071 and 93G047).

References and Notes

(1) Fendler, J. H.; Fendler, E. J. *Catalysis in Micellar and Macromolecular Systems*; Academic Press: New York, 1975.
(2) Stenius, P. In *Reversed Micelles*, Luisi, P. L., Straub, B. E., Eds.; Plenum Press: New York, 1984.
(3) Langevin, D. In *Structure and Reactivity in Reversed Micelles*; Pileni, M. P., Ed., Elsevier: Amsterdam, 1989.
(4) Ekwall, P. *Adv. Liq. Cryst.* **1975**, *1*, 1.
(5) Tamamushi, B.; Watanabe, N. *Colloid Polym. Sci.* **1980**, *258*, 174.
(6) Peyrelasse, J. B.; Boned, C. *J. Phys. Chem.* **1985**, *89*, 370.
(7) See for instance: *Neutrons in Biology*; Schoenborn, B. P., Ed.; Plenum Press: New York, 1984.
(8) Higgins, J. S.; Maconnachie, A. In *Methods of Experimental Physics*; Skld, K., Price, D. L., Eds.; Academic Press: New York, 1987; Vol. 23, Part C, p 287.
(9) Feigin, L. A.; Svergun, D. I. In *Structure Analysis by Small-Angle X-ray and Neutron Scattering*; Taylor, G. W., Ed.; Plenum Press: New York, 1987.
(10) Stuhrmann, H. B. *Physica B* **1989**, *156/157*, 444.
(11) See for instance: *Neutron, X-ray and Light Scattering*; Lindner, P., Zemb, Th., Eds.; Elsevier: Amsterdam, 1991.
(12) Geyer, A. D.; Tabony, J. *Chem. Phys. Lett.* **1985**, *113*, 83.
(13) Howe, A. M.; Toprakcioglu, C.; Dore, J. C.; Robinson, B. H. *J. Chem. Soc., Faraday Trans. 1* **1986**, *82*, 2411.
(14) Sheu, E.; Göklen, K. E.; Hatton, T. A.; Chen, S. H. *Biotech. Prog.* **1986**, *2*, 175.
(15) Caponetti, E.; Magid, L. J. *Langmuir* **1986**, *2*, 722.
(16) North, A. N.; Dore, J. C.; Mcdonald, J. A.; Robinson, B. H.; Heenan, R. K.; Howe, A. M. *Colloids Surf.* **1986**, *19*, 21.
(17) Teubner, M.; Strey, R. *J. Chem. Phys.* **1987**, *87*, 3195.
(18) Rahaman, R. S.; Hatton, T. A. *J. Phys. Chem.* **1991**, *95*, 1799.

(19) Eastoe, J.; Fragneto, G.; Robinson, B. H.; Towey, T. F.; Heenan, R. K.; Leng, F. J. *J. Chem. Soc., Farady Trans.* **1992**, *88*, 461.

(20) Robertus, C.; Joosten, J. G. H.; Levine, Y. K. *J. Chem. Phys.* **1990**, *94*, 7293.

(21) Pileni, M. P.; Zemb, T.; Petit, C. *Chem. Phys. Lett.* **1985**, *118*, 414.

(22) Pileni, M. P. *J. Phys. Chem.* **1993**, *97*, 6961.

(23) Ueki, T.; Hiragi, Y.; Kataoka, M.; Inoko, Y.; Amemiya, Y.; Izumi, Y.; Tagawa, H.; Muroga, Y. *Biophys. Chem.* **1985**, *23*, 115.

(24) Stuhrmann, H. B.; Kirste, R. G. *Z. Phys. Chem.* **1965**, *46*, 247.

(25) Porod, G. *Kolloid Z.* **1951**, *124*, 251.

(26) Daoud, M.; Joanny, J. F. I. *Physis (Paris)* **1981**, *42*, 1359.

(27) Witten, T. A.; Sander, L. M. *Phys. Rev. Lett.* **1981**, *47*, 1400.

(28) Meakin, P. *Phys. Rev. Lett.* **1983**, *51*, 1119.

(29) Bale, H. D.; Schmidt, P. W. *Phys. Rev. Lett.* **1984**, *53*, 596.

(30) Schaefer, D. W.; Keefer, K. D. *Phys. Rev. Lett.* **1986**, *56*, 2199.

(31) Keefer, K. D.; Schaefer, D. W. *Phys. Rev. Lett.* **1986**, *56*, 2376.

(32) Kriste, R. G.; Oberthür, R. C. In *Small Angle X-ray Scattering*; Glatter, O., Kratky, O., Eds.; Academic Press: London, 1982.

(33) Glatter, O. In *Small Angle X-ray Scattering*; Glatter, O., Kratky, O., Eds.; Academic Press: London, 1982.

(34) Hirai, M.; Kawai-Hirai, R.; Hirai, T.; Ueki, T. *Eur. J. Biochem.* **1993**, *215*, 55.

(35) Hirai, M.; Hirai, T.; Ueki, T. *Macromolecules* **1994**, *27*, 1003.

(36) Israelachvili, J. N.; Mitchell, D. J.; Ninham, B. W. *J. Chem. Soc., Farady Trans. 2* **1976**, *72*, 1525.

(37) Israelachvili, J. N.; Mitchell, D. J.; Ninham, B. W. *Biochim. Biophys. Acta* **1977**, *470*, 185.

(38) Mitchell, D. J.; Ninham, B. W. *J. Chem. Soc., Faraday Trans. 2* **1981**, *77*, 601.

(39) Kotlarchyk, M.; Huang, J. S.; Chen, S. H. *J. Phys. Chem.* **1985**, *89*, 4382.

(40) Huang, J. S.; Safran, S. A.; Kim, M. W.; Grest, G. S. Kotlarchyk, M.; Quirke, N. *Phys. Rev. Lett.* **1984**, *53*, 592.

(41) Robertus, C.; Philipse, W. H.; Joosten, J. G. H.; Levine, Y. K. *J. Chem. Phys.* **1989**, *90*, 4482.

(42) Eastoe, J.; Steytler, D. C.; Robinson, B. H.; Heenan, R. K.; North, N. A.; Dore, C. J. *J. Chem. Soc., Faraday Trans.* **1994**, *90*, 85.

(43) Hirai, M.; Kawai-Hirai, R.; Nakamura, K.; Takizawa, T.; Yabuki, S.; Kobayashi, K.; Ameniya, Y.; Oya, M. *J. Chem. Soc., Faraday Trans.*, in press.

JP942767H